Available online at www.sciencedirect.com
SCIENCE DIRECT®
International Journal of Heat and Mass Transfer 48 (2005) 5460–5474
International Journal of HEAT and MASS TRANSFER
www.elsevier.com/locate/ijhmt

Enhancement of heat transfer: Combined convection and radiation in the entrance region of circular ducts with porous inserts

Xuelei Chen [a], William H. Sutton [b,*]

[a] Simulation Technology Solutions, John Zink Company LLC, Tulsa, OK 74116, USA
[b] Department of Mechanical Engineering, University of Alabama, Tuscaloosa, AL 35487, USA

Received 11 July 2004; received in revised form 24 June 2005
Available online 24 August 2005

Abstract

Using porous ceramic inserts in high temperature equipment has been proven to be an effective means to enhance combined convective–radiative heat transfer. The porous ceramic insert was referred to as a convection-to-radiation converter (CRC) by previous investigators. We consider a novel application of CRC cores in a partial by pass flow system for heat transfer enhancement. Both hydrodynamically and thermally developing laminar flow is considered in the entrance region of a circular pipe with a porous insert located at the center. The momentum and Darcy–Brinkman equations are applied to the flow field in the annular gas layer and central porous layer respectively. The energy equation is coupled with the radiative transfer equation by the radiation source term. The radiative transfer is simulated by the newly developed integral equations [X.L. Chen, W. Sutton, Radiative transfer in finite cylindrical media using transformed integral equations, J. Quant. Spectrosc. Radiat. Transfer 77 (3) (2003) 233–271; W. Sutton, X.L. Chen, A general integration method for radiative transfer in 3-D non-homogeneous cylindrical media with anisotropic scattering, J. Quant. Spectrosc. Radiat. Transfer 84 (2004) 65–103] to avoid singularity problem and give high accuracy. The working fluid and porous medium are both considered as participating media. Finally, this highly nonlinear system of equations is solved by a mixed iteration method. The results are compared between the cases with and without the porous insert. The porous insert enhances both convective and radiative transfer by about 35% and 105% respectively at the most. The effects of important parameters on this enhancement are discussed in detail.

1. Introduction

Over the years, porous materials have found important applications in high temperature thermal energy systems, where the convection and radiation modes of heat transfer are both important. The purpose for this promising technique is to use porous medium to enhance combined convective–radiative transfer, to save remarkable energy, or to keep heat from releasing from high temperature areas for combustion requirements in various industrial furnaces, combustors, and incinerators.

For the purpose of enhancing combined convective–radiative heat transfer, the earliest investigators [1–3]

* Corresponding author.
E-mail address: wsutton@coe.eng.ua.edu (W.H. Sutton).

0017-9310/$ - see front matter © 2005 Elsevier Ltd. All rights reserved.
doi:10.1016/j.ijheatmasstransfer.2005.06.025

Nomenclature

a	coefficients of discretization equations, or linear anisotropic scattering coefficient
A	differential surface area, m^2
Bo	Boltzmann number, $Bo = \frac{\rho \cdot C_p u_{in}}{n^2 \sigma T_{in}^3}$
C_p	constant pressure specific heat, J/(kg K)
Da	Darcy number, $Da = \frac{K}{R_{out}^2}$
e	coefficient related to externally incident radiation and defined in Eq. (14d)
G	incident radiation, W/m^2
I	the intensity of radiation, W/m^2
k	thermal conductivity, W/(m K)
K	permeability, m^2
L	the pipe length, m
Nu	Nusselt number, $Nu_T = \frac{q_w D_{out}}{k(T_b - T_w)}$
p	pressure, N/m^2
Pr	Prandtl number, $Pr = \frac{\mu \cdot C_p}{k}$
q	heat flux, or components of net radiative heat flux, W/m^2
Re	Reynolds number, $Re = \frac{\rho \cdot u_{in} R_{out}}{\mu}$
R	the radius, m
S	source term, W/m^2
T	temperature, K
u	velocity in z-direction, m/s
v	velocity in r-direction, m/s

Greek symbols

α	a specified angle in the transformed coordinate
β	extinction coefficient, 1/m
ε	the surface emissivity
θ	dimensionless temperature, or angle between surface normal vector and the intensity
γ	the specified distance in the transformed coordinate
μ	absolute viscosity, N s/m^2
ρ	density kg/m^3, or surface reflectivity
τ	optical thickness
φ	porosity
ξ	an adjustable parameter in the stress jump condition
χ	a specified angle in the transformed coordinate
ω	single scattering albedo
Ω	the unit vector in the intensity direction, or the solid angle

Superscript

–	non-dimensional quantity

Subscripts

b	black body, or bulk
e	effective
f	fluid
in	inlet, or inside porous domain
out	outlet, or outside fluid domain
r	radial direction
z	axial direction
w	wall

like Mori et al. suggested adding parallel plates in high temperature gas side of heat exchangers. The plates receive heat energy from the gas by convection, and then emit radiation to the colder absorbing surface. The metal emissivity is much higher than gas emissivity; more heat can be recaptured by the absorbing surface. Later Echigo [4] proposed to improve the enhancement effect by using porous segment placed normal to the flow direction. Since porous materials have a large surface area per unit volume and a much stronger radiation emittance than gas media does, much more energy is emitted by the porous segments mainly back to the upstream direction and cause the temperature to drop sharply along flow direction. His numerical analysis was based on the assumptions of non-radiating gas, non-scattering porous medium, and one-dimensional simplification. Zhang et al. [5] proposed and solved a fully developed duct flow with a porous core in the center (partial blockage for reduced pressure drop). They performed numerical analysis and results proved the efficiency of porous core in the enhancement of combined heat transfer. The essential assumption was fully developed flow, also no considerations to the inlet and outlet radiative effects.

This study proposes a similar application of the porous core to [5]. But many realistic factors are considered to simulate combined convection–radiation in the entrance region, which is numerically solved by control volume method for both flow and temperature fields. The Brinkman type extension of the Darcy law and Navier–Stokes equation are used to solve the velocity field in the porous and fluid layers respectively. The newly developed integral equations of radiative transfer [6,7] are used to simulate radiation in the emitting, absorbing, and anisotropically scattering gas and porous media. Finally, the effects of upstream emissivity, downstream emissivity, Reynolds number, extinction coefficients, scattering albedo and Darcy number are presented and discussed in detail. This non-linear system is believed to be useful for other application systems.

2. Governing equations

Geometry consideration consists of a circular duct or pipe as shown in Fig. 1(a). A porous core is concentrically inserted in pipe with radius R_m. The hot participating gas enters the pipe with uniform velocity u_{in} and temperature T_{in} and is cooled by the cold wall at constant temperature T_w. Both the fluid and porous matrix are assumed to have constant properties. We consider axisymmetric, laminar, boundary-layer flow and neglect axial rate of change of viscous stress. If following dimensionless variables and parameters are introduced

$$\bar{r}=\frac{r}{R_{out}},\quad \bar{z}=\frac{z}{R_{out}},\quad \bar{u}=\frac{u}{u_{in}},\quad \bar{v}=\frac{v}{u_{in}},$$
$$\theta=\frac{T}{T_{in}},\quad \bar{p}=\frac{p}{\rho\cdot u_{in}^2},\quad Re=\frac{\rho\cdot u_{in}R_{out}}{\mu},$$
$$Pr=\frac{\mu\cdot C_p}{k},\quad Da=\frac{K}{R_{out}^2},\quad Bo=\frac{\rho\cdot C_p u_{in}}{n^2\sigma T_{in}^3},$$
$$\overline{G}=\frac{G}{\sigma T_{in}^4},\quad \bar{q}_r=\frac{q_r}{\sigma T_{in}^4},\quad \bar{q}_z=\frac{q_z}{\sigma T_{in}^4},$$
$$\bar{I}=\frac{I}{\sigma T_{in}^4},\quad \bar{\beta}=\beta\cdot R_{out} \tag{1}$$

governing equations of fluid and porous regions reduce to following non-dimensional forms:

Continuity equation

Fluid region
$$\frac{1}{\bar{r}}\cdot\frac{\partial(\bar{r}\cdot\bar{v})}{\partial\bar{r}}+\frac{\partial\bar{u}}{\partial\bar{z}}=0, \tag{2a}$$

Porous region
$$\frac{1}{\bar{r}}\cdot\frac{\partial(\bar{r}\cdot\bar{v})}{\partial\bar{r}}+\frac{\partial\bar{u}}{\partial\bar{z}}=0. \tag{2b}$$

Momentum equation

Fluid region
$$\frac{1}{\bar{r}}\frac{\partial(\bar{r}\bar{u}\bar{v})}{\partial\bar{r}}+\frac{\partial(\bar{u}\bar{u})}{\partial\bar{z}}=-\frac{d\bar{p}}{d\bar{z}}+\frac{1}{Re}\left[\frac{1}{\bar{r}}\frac{\partial}{\partial\bar{r}}\left(\bar{r}\frac{\partial\bar{u}}{\partial\bar{r}}\right)\right], \tag{3a}$$

Porous region
$$\frac{1}{\bar{r}}\frac{\partial(\bar{r}\bar{u}\bar{v})}{\partial\bar{r}}+\frac{\partial(\bar{u}\bar{u})}{\partial\bar{z}}=-\varphi\frac{d\bar{p}}{d\bar{z}}-\varphi\frac{1}{Re\cdot Da}\bar{u}+\frac{1}{(Re)_e}\left[\frac{1}{\bar{r}}\frac{\partial}{\partial\bar{r}}\left(\bar{r}\frac{\partial\bar{u}}{\partial\bar{r}}\right)\right]. \tag{3b}$$

Energy equation

Fluid region
$$\frac{1}{\bar{r}}\frac{\partial(\bar{r}\bar{v}\theta)}{\partial\bar{r}}+\frac{\partial(\bar{u}\theta)}{\partial\bar{z}}=\frac{1}{RePr}\left[\frac{1}{\bar{r}}\frac{\partial}{\partial\bar{r}}\left(\bar{r}\frac{\partial\theta}{\partial\bar{r}}\right)+\frac{\partial^2\theta}{\partial\bar{z}^2}\right]+\frac{\bar{\beta}(1-\omega)}{Bo}(\overline{G}-4\theta^4), \tag{4a}$$

Porous region
$$\frac{1}{\bar{r}}\frac{\partial(\bar{r}\bar{v}\theta)}{\partial\bar{r}}+\frac{\partial(\bar{u}\theta)}{\partial\bar{z}}=\frac{1}{(Re)_e(Pr)_e}\left[\frac{1}{\bar{r}}\frac{\partial}{\partial\bar{r}}\left(\bar{r}\frac{\partial\theta}{\partial\bar{r}}\right)+\frac{\partial^2\theta}{\partial\bar{z}^2}\right]+\frac{\bar{\beta}(1-\omega)}{Bo}(\overline{G}-4\theta^4). \tag{4b}$$

In dimensionless variables, u and v are velocity components in z or r direction respectively as shown in Fig. 1(a). The subscript e means effective properties of porous media. In $(Re)_e$ and $(Pr)_e$ numbers, μ_e and k_e are used, which are effective viscosity and conductivity of the porous insert. The Einstein formula can be used

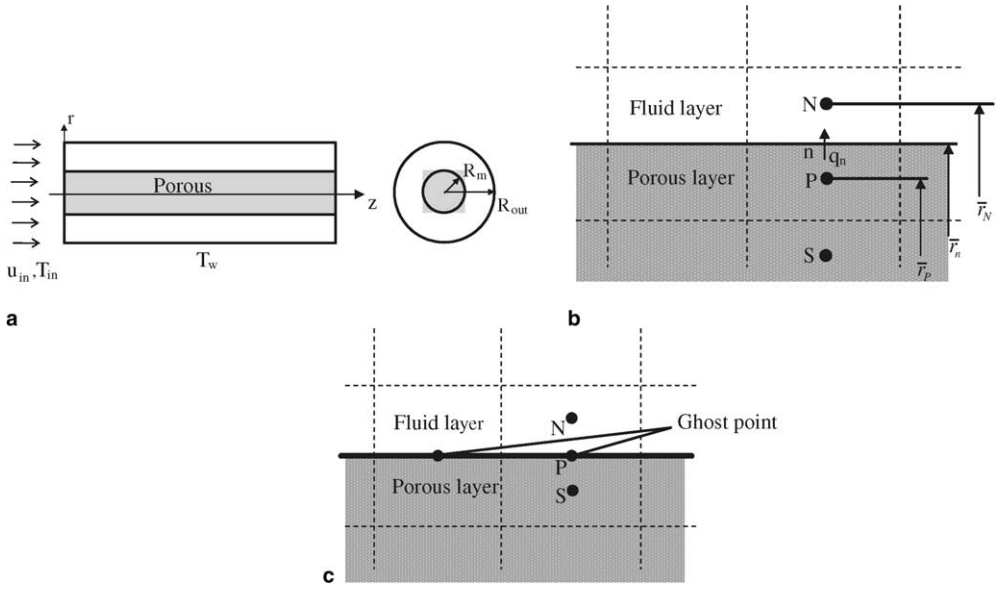

Fig. 1. Schematic illustration of the flow system. (a) Schematic diagram of the flow system and coordinates; (b) Illustration of the heat flux at the fluid–porous interface; (c) Illustration of the 'ghost' points at the fluid–porous interface.

to obtain μ_e, but in this work, we assume $\mu_e = \mu$ [8]. The following equation is used to compute k_e:

$$k_e = \varphi \cdot k_f + (1-\varphi)k_s, \tag{5}$$

where k_f, k_s is the conductivity of fluid or solid material of the porous insert respectively. The inertial term is not considered in Eq. (3b). When certain length scale constraints are satisfied, Darcy's law with the first Brinkman correction without inertial effects is derived for homogeneous porous region [9,10]. Also this inertial effect is found to be insignificant in [11]. The last terms in the energy equations are contributions of thermal radiation and are dimensionless expressions of the negative value of the divergence of net radiative heat flux, which can be computed for gray radiation by the following relation:

$$-\nabla \cdot \vec{q}_R = \beta(1-\omega)(G - 4n^2\sigma T^4), \tag{6}$$

where $\vec{q}_R$ is the net radiative heat flux; n is the refractive index, which is assumed as one.

Due to the boundary-layer flow simplifications, the radial momentum equation has been neglected. Instead, we use the integrated mass conservation equation to complete the problem:

$$\int_0^1 2\pi\bar{r}\bar{u}\cdot \mathrm{d}\bar{r} = \pi. \tag{7}$$

For momentum and energy equations, the dimensionless boundary conditions are

$$\begin{aligned}
&\text{At inlet boundary } \bar{z}=0\text{:}\\
&\quad \bar{u}=1, \quad \bar{v}=0, \quad \theta=1.\\
&\text{At outlet boundary } \bar{z}=\frac{L}{R_{out}}\text{:}\\
&\quad \text{outflow boundary condition.}\\
&\text{At centerline } \bar{r}=0\text{:}\\
&\quad \frac{\partial \bar{u}}{\partial \bar{r}}=0, \quad \frac{\partial \theta}{\partial \bar{r}}=0.\\
&\text{At interface } \bar{r}=\overline{R}_m=\frac{R_m}{R_{out}}\text{:}\\
&\quad \bar{u}_{fluid}=\bar{u}_{porous}, \quad \frac{1}{Re}\frac{\partial \bar{u}_{fluid}}{\partial \bar{r}}=\frac{1}{Re_e}\frac{\partial \bar{u}_{porous}}{\partial \bar{r}},\\
&\quad \theta_{fluid}=\theta_{porous}, \quad \frac{1}{RePr}\frac{\partial \theta_{fluid}}{\partial \bar{r}}=\frac{1}{(Re)_e(Pr)_e}\frac{\partial \theta_{porous}}{\partial \bar{r}}\\
&\text{At outside wall } \bar{r}=1\text{:}\\
&\quad \bar{u}=\bar{v}=0, \quad \theta=\theta_w=\frac{T_w}{T_{in}}.
\end{aligned} \tag{8}$$

where the outflow boundary condition is that the region near the outflow boundary exhibits local one-way behavior when Peclet number is sufficiently large [12]. At the fluid–porous interface, non-jump condition is used. But the stress jump condition has been recognized [9]. Good agreement with experiment was achieved by a single adjustable parameter that appears in the extra term of the jump condition [10]. The effects of the parameter will be discussed later.

2.1. Radiative transfer equation (RTE)

In order to obtain source terms included in energy equations, we have to consider the radiative transfer equation. We use the newly developed integral equations [6,7] to calculate incident radiation and components of the net heat flux. We know that the incident radiation and heat flux at a particular point can be evaluated by the integration of the intensity at that point over full 4π solid angle. In axisymmetric 2-D cylindrical coordinate system [7],

$$\overline{G}(\bar{z},\bar{r}) = \int_{4\pi} \bar{I}(\bar{z},\bar{r},\hat{\Omega})\cdot \mathrm{d}\Omega, \tag{9a}$$

$$\bar{q}_r(\bar{z},\bar{r}) = \int_{4\pi} \bar{I}(\bar{z},\bar{r},\hat{\Omega})\cdot \cos(\hat{e}_r,\hat{\Omega})\cdot \mathrm{d}\Omega, \tag{9b}$$

$$\bar{q}_z(\bar{z},\bar{r}) = \int_{4\pi} \bar{I}(\bar{z},\bar{r},\hat{\Omega})\cdot \cos(\hat{e}_z,\hat{\Omega})\cdot \mathrm{d}\Omega, \tag{9c}$$

where $\bar{q}_r$, $\bar{q}_z$ are components of the net heat flux. $\bar{I}(\bar{z},\bar{r},\hat{\Omega})$ is the intensity at position $s(\bar{z},\bar{r})$ and in $\hat{\Omega}$ direction,

$$\bar{I}(\bar{z},\bar{r},\hat{\Omega}) = \bar{I}_i \exp\left[-\tau(s_i,s)\right] + \int_{s_i}^{s} \bar{\beta}(s')\overline{S}(s',\hat{\Omega}) \times \exp\left[-\tau(s',s)\right]\cdot \mathrm{d}\bar{s}', \tag{10}$$

where s_i is the boundary point, $\hat{\Omega}$ is the ray direction from start point s_i to end point s, and s' is the intermediate point between s_i and s. $\bar{I}_i$ is the entering intensity at boundary i ($i=1$, 2, 3 for inlet, outlet, and outside boundary respectively). The above equation is the formal solution of the RTE [13]. The source term in above equation can be expressed as follows if the linear-anisotropic scattering phase function is assumed:

$$\overline{S} = (1-\omega)\bar{I}_b(\theta) + \frac{\omega}{4\pi}\left\{\overline{G}(\bar{z},\bar{r}) + a_1\left[\bar{q}_r(\bar{z},\bar{r})\cos(\hat{e}_r,\hat{\Omega}) + \bar{q}_z(\bar{z},\bar{r})\cos(\hat{e}_z,\hat{\Omega})\right]\right\}, \tag{11}$$

where

$$\bar{I}_b(\theta) = \frac{\theta^4}{\pi}. \tag{12}$$

The optical thickness in Eq. (10) is defined by

$$\tau(s_i,s) = \int_{s_i}^{s}\beta(s')\,\mathrm{d}s' = \int_{s_i}^{s}\bar{\beta}(s')\frac{\mathrm{d}s'}{R_{out}} = \int_{s_i}^{s}\bar{\beta}(s')\,\mathrm{d}\bar{s}'. \tag{13}$$

The radiative boundary conditions are:

At inlet $\bar{z}=0$, transparent boundary:

$$\bar{I}_1(0,\bar{r}) = \bar{f}_1 = \frac{f_1(r)}{\sigma T_{in}^4}, \tag{14a}$$

At outlet $\bar{z} = \dfrac{L}{R_{\text{out}}}$, transparent boundary:

$$\bar{I}_2(\bar{L}, \bar{r}) = \bar{f}_2 = \frac{f_2(r)}{\sigma T_{\text{in}}^4}, \tag{14b}$$

At the opaque wall $\bar{r} = 1$:

$$\bar{I}_3(\bar{z}, 1) = \frac{\varepsilon_{\text{w}} \theta_{\text{w}}^4}{\pi} + \frac{\rho_{\text{w}}}{\pi} \int_{2\pi} \bar{I}(\bar{z}, 1) \cos(\hat{e}_r, \hat{\Omega}) \, \mathrm{d}\Omega, \tag{14c}$$

where f_1 and f_2 are possible externally incident radiations at the inlet and outlet. In order to be compatible with temperature boundary conditions, we assume they can be expressed in the form:

$$f_1 = e_1 \left(\frac{\sigma T_{\text{in}}^4}{\pi} \right), \quad f_2 = e_2 \left[\frac{\sigma T^4(L, r)}{\pi} \right], \tag{14d}$$

where the coefficients e_1 and e_2 are between $[0, 1]$ in order to be compatible with different actual situations, for example colder source temperature. Most investigators assume upstream and downstream incoming radiation as black body source at inlet and outlet temperature, that is e_1 and e_2 are assumed to be 1.0 in the above equations. Assuming e_1 and e_2 equal to 1.0 may strongly affect the analysis results, as indicated below.

The inlet and exit boundary conditions for radiative heat transfer depend on a number of factors. If a region up or downstream beyond the porous insert is large, in comparison to the adjacent area normal to the flow, while the gas is radiatively transparent, then the incident radiation will appear to originate from radiatively black walls. This could result in a colder temperature radiatively than the continuous average inlet or exit gas temperature. If the same external relatively large (in comparison to the flow area) region has a luminous combustion or an optically thick gas, then the condition will appear as radiatively black at the gas temperature. If the same region is of the same order of size as the flow area while the walls are not black (for example refractory brick) or the gas is semi-transparent, then the up or downstream radiative problem must be solved prior to input to the current combined problem. Here, the radiation is specified as an incident radiative intensity at either end of the duct being analyzed. Thus, any of the conditions above can be replicated. When both e_1 and e_2 equal to 1.0, we have the maximum externally incident radiations.

3. Numerical methods

Because the momentum equations, energy equations and radiative transfer equation are solved by different numerical techniques, the flow-heat transfer problem and radiative transfer problem are treated separately in the following sections.

3.1. Numerical method for momentum and energy equations

CFD control volume method is used to get discretization equations of momentum and energy equations. The computing domain is divided into a number of non-overlapping control volumes (CV) and each differential equation is integrated over the control volume. The staggered grids and the power-law scheme are adopted. The two-dimensional discretization equation may be expressed at a point P in terms of adjacent East, West, South and North neighbors:

$$a_{\text{P}} \Phi_{\text{P}} = a_{\text{E}} \Phi_{\text{E}} + a_{\text{W}} \Phi_{\text{W}} + a_{\text{S}} \Phi_{\text{S}} + a_{\text{N}} \Phi_{\text{N}} + b, \tag{15}$$

where Φ could be dimensionless velocity $\bar{u}$ or temperature θ. The coefficients are determined by F, D, and P, which are the strength of convection, the diffusion conductance, and Peclet number of that CV [12]. The coefficients are also determined by the source term. For momentum equations, source terms in fluid region and porous region are expressed by

$$S_{\text{fluid}} = \frac{\bar{p}_{\text{w}} - \bar{p}_{\text{e}}}{\Delta \bar{z}}, \quad S_{\text{porous}} = \frac{\varphi(\bar{p}_{\text{w}} - \bar{p}_{\text{e}})}{\Delta \bar{z}} - \frac{\varphi}{ReDa} \bar{u}_{\text{p}}. \tag{16a, b}$$

For energy equations, the source term expression in porous region is the same as in fluid region:

$$S = \frac{\bar{\beta}(1 - \omega)}{Bo} (\overline{G} + 12\theta^{*4}) - \frac{16\bar{\beta}(1 - \omega)}{Bo} \theta^{*3} \theta_P, \tag{17}$$

where θ^* is the previous iteration value of θ. To bring the problem to closure, the total mass conservation equation (7) is used to get a pressure correction equation.

The computation domain includes fluid and porous regions, so obtaining a good representation for the heat flux at the interface is important to get the correct solution. There are two kinds of grid schemes to deal with this difficulty. One is shown in Fig. 1(b) and another is shown in Fig. 1(c). In Fig. 1(b), control volume face n locates exactly on the interface, we have the harmonic diffusion coefficient expressed as

$$\Gamma_n = \frac{\ln(\bar{r}_N / \bar{r}_P)}{\frac{\ln(\bar{r}_n / \bar{r}_P)}{\Gamma_P} + \frac{\ln(\bar{r}_N / \bar{r}_n)}{\Gamma_N}}, \tag{18}$$

where Γ represents conductivity and viscosity in energy and momentum equations respectively.

3.2. Numerical method for radiative transfer equations

The interface for thermal radiation is assumed free and non-reflecting. The medium is enclosed by three bounding surfaces i ($i = 1, 2, 3$). The solid angle integration for incident radiation and heat fluxes could be transformed to surface integrations:

$$\overline{G}(\bar{z},\bar{r}) = \sum_{i=1}^{3} \iint_i \bar{I}(\bar{z},\bar{r},\hat{\Omega}) \cdot \frac{\cos\theta_i}{\bar{d}^2(s_i,s)} \mathrm{d}\bar{A}_i, \tag{19a}$$

$$\bar{q}_r(\bar{z},\bar{r}) = \sum_{i=1}^{3} \iint_i \bar{I}(\bar{z},\bar{r},\hat{\Omega}) \cdot \cos(\hat{e}_r,\hat{\Omega}) \frac{\cos\theta_i}{\bar{d}^2(s_i,s)} \mathrm{d}\bar{A}_i, \tag{19b}$$

$$\bar{q}_z(\bar{z},\bar{r}) = \sum_{i=1}^{3} \iint_i \bar{I}(\bar{z},\bar{r},\hat{\Omega}) \cdot \cos(\hat{e}_z,\hat{\Omega}) \frac{\cos\theta_i}{\bar{d}^2(s_i,s)} \mathrm{d}\bar{A}_i, \tag{19c}$$

where θ_i is the angle between the unit normal vector $\hat{n}_i$ of surface i and the intensity direction $\hat{\Omega}$. Cosines are referred to [6,7]. The term $\bar{d}(s_i,s)$ is the dimensionless distance from point $s_i(\bar{z}_i,\bar{r}_i,\phi_i)$ on the boundary i to point $s(\bar{z},\bar{r},\phi)$ in the medium.

$$\bar{d}(s_i,s) = \left[\bar{r}_i^2 + \bar{r}^2 - 2\bar{r}_i\bar{r}\cos(\phi-\phi_i) + (\bar{z}-\bar{z}_i)^2\right]^{1/2}. \tag{20}$$

For 2-D problem, ϕ vanishes. Please note that the surface integration involves only the geometry. Radiation properties augment the calculation of the intensity.

To calculate surface integrations easier and without singularity near boundaries, we transfer the coordinate $(\bar{z}_i,\bar{r}_i,\phi_i)$ $(i=1,2,3)$ of integration to a new coordinate (α,γ,χ) system [6,7]. By doing so, we have

$$\begin{aligned}\overline{G}(\bar{z},\bar{r}) = &\int_{-\pi}^{\pi}\int_0^{\gamma_R} \frac{\bar{I}}{\gamma}(-\sin\alpha_1)\cos^2\alpha_1 \,\mathrm{d}\gamma\,\mathrm{d}\chi \\ &+ \int_{-\pi}^{\pi}\int_0^{\gamma_R} \frac{\bar{I}}{\gamma}\sin\alpha_2\cos^2\alpha_2 \,\mathrm{d}\gamma\,\mathrm{d}\chi \\ &+ \int_{-\pi}^{\pi}\int_{\alpha_1}^{\alpha_2} \bar{I}\cdot\cos\alpha\cdot\mathrm{d}\alpha\,\mathrm{d}\chi,\end{aligned} \tag{21a}$$

$$\begin{aligned}\bar{q}_r(\bar{z},\bar{r}) = &\int_{-\pi}^{\pi}\int_0^{\gamma_R} \frac{\bar{I}}{\gamma}\sin\alpha_1\cos^3\alpha_1\cos\chi \,\mathrm{d}\gamma\,\mathrm{d}\chi \\ &+ \int_{-\pi}^{\pi}\int_0^{\gamma_R} \frac{\bar{I}}{\gamma}\sin\alpha_2\cos^3\alpha_2(-\cos\chi) \,\mathrm{d}\gamma\,\mathrm{d}\chi \\ &+ \int_{-\pi}^{\pi}\int_{\alpha_1}^{\alpha_2} \bar{I}\cdot\cos^2\alpha(-\cos\chi)\,\mathrm{d}\alpha\,\mathrm{d}\chi,\end{aligned} \tag{21b}$$

$$\begin{aligned}\bar{q}_z(\bar{z},\bar{r}) = &\int_{-\pi}^{\pi}\int_0^{\gamma_R} \frac{\bar{I}}{\gamma}\sin^2\alpha_1\cos^2\alpha_1 \,\mathrm{d}\gamma\,\mathrm{d}\chi \\ &+ \int_{-\pi}^{\pi}\int_0^{\gamma_R} \frac{\bar{I}}{\gamma}(-1)\sin^2\alpha_2\cos^2\alpha_2 \,\mathrm{d}\gamma\,\mathrm{d}\chi \\ &+ \int_{-\pi}^{\pi}\int_{\alpha_1}^{\alpha_2} \bar{I}\cdot(-\sin\alpha)\cos\alpha\cdot\mathrm{d}\alpha\,\mathrm{d}\chi,\end{aligned} \tag{21c}$$

where

$$\gamma_R = \sqrt{\overline{R}_{out}^2 - \bar{r}^2\sin^2\chi} - \bar{r}\cos\chi, \tag{22}$$

$$\alpha_1 = \arctan\frac{0-\bar{z}}{\gamma}, \quad \alpha_2 = \arctan\frac{\bar{L}-\bar{z}}{\gamma}. \tag{23a, b}$$

Once the new coordinate (α,γ,χ) is known, the old coordinate $(\bar{z}_i,\bar{r}_i,\phi_i)$ can be obtained [6,7]. The old coordinate $(\bar{z}_i,\bar{r}_i,\phi_i)$ is needed in computing the intensity.

3.3. The intensity

Considering a radiative ray along the path starting from point $s_i(\bar{z}_i,\bar{r}_i,\phi_i)$ to point $s(\bar{z},\bar{r},\phi)$, the radiation intensity is computed by Eq. (10). Here we have two layers with different properties, so we need to integrate by segments. A step-change extinction coefficient and scattering albedo are assumed in the radial direction as follows:

$$\beta(\bar{z}',\bar{r}') = \beta_{in} = \beta_{porous}, \quad \omega(\bar{z}',\bar{r}') = \omega_{in} = \omega_{porous}, \quad \text{when } 0 \leqslant \bar{r}' \leqslant \overline{R}_m, \tag{24a}$$

$$\beta(\bar{z}',\bar{r}') = \beta_{out} = \beta_{fluid}, \quad \omega(\bar{z}',\bar{r}') = \omega_{out} = \omega_{fluid}, \quad \text{when } \overline{R}_m \leqslant \bar{r}' \leqslant \overline{R}_{out}. \tag{24b}$$

If the line $\overline{s_i s}$ across these two layers, the intensity from start point $s_i(\bar{z}_i,\bar{r}_i,\phi_i)$ to point $s(\bar{z},\bar{r},\phi)$ will go through different layers. The position of intersection is required.

If any point $s'(\bar{z}',\bar{r}',\phi')$ lays on the line $\overline{s_i s}$, then

$$\bar{z}' = \bar{z}_i + (\bar{z}-\bar{z}_i)\cdot t, \quad \bar{r}' = \sqrt{\bar{x}'^2+\bar{y}'^2}, \tag{25a, b}$$

where

$$\bar{x}' = \bar{x}_i + (\bar{x}-\bar{x}_i)\cdot t = \bar{r}_i\cos\phi_i + (\bar{r}\cos\phi - \bar{r}_i\cos\phi_i)\cdot t, \tag{25c}$$

$$\bar{y}' = \bar{y}_i + (\bar{y}-\bar{y}_i)\cdot t = \bar{r}_i\sin\phi_i + (\bar{r}\sin\phi - \bar{r}_i\sin\phi_i)\cdot t, \tag{25d}$$

where $1 \geqslant t \geqslant 0$. The intersection point of the line and the circle $\bar{r} = \overline{R}_m$ is solved for t as:

$$t_{1,2} = \frac{\bar{r}_i[\bar{r}_i - \bar{r}\cos(\phi-\phi_i)] \pm \sqrt{\bar{r}_i^2[\bar{r}_i-\bar{r}\cos(\phi-\phi_i)]^2 + \gamma^2(\overline{R}_m^2 - \bar{r}_i^2)}}{[\bar{r}^2 + \bar{r}_i^2 - 2\bar{r}\bar{r}_i\cos(\phi-\phi_i)]}. \tag{26}$$

In above equation, the '−' operation in the numerator goes with solution t_1 and the '+' operation goes with solution t_2. So the root t_2 is always greater than t_1. From systematic analysis of $t_{1,2}$ equation, we have following possibilities:

If $\bar{r} \leqslant \overline{R}_m$ (for schematic diagram, refer [7])

(1) When t_1, $t_2 \notin [0, 0.1]$.

$$\begin{aligned}\bar{I}(\bar{z},\bar{r},\hat{\Omega}) = &\bar{I}_i \exp[-\bar{\beta}_{in}\bar{d}(s_i,s)] \\ &+ \int_0^1 \bar{\beta}_{in}\overline{S}(\omega_{in})\exp[-\bar{\beta}_{in}(1-t)\bar{d}(s_i,s)] \\ &\times \bar{d}(s_i,s)\,\mathrm{d}t.\end{aligned} \tag{27a}$$

(2) When only $t_1 \in [0,1]$.

$$\begin{aligned}\bar{I}(\bar{z},\bar{r},\hat{\Omega}) &= \bar{I}_i \exp\left\{-[\bar{\beta}_{\text{out}} t_1 + \bar{\beta}_{\text{in}}(1-t_1)]\bar{d}(s_i,s)\right\} \\ &+ \int_0^{t_1} \bar{\beta}_{\text{out}}\overline{S}(\omega_{\text{out}}) \exp\left\{-[\bar{\beta}_{\text{out}}(t_1-t) \right. \\ &\left. +\bar{\beta}_{\text{in}}(1-t_1)]\bar{d}(s_i,s)\right\}\bar{d}(s_i,s)\,\mathrm{d}t + \int_{t_1}^{1} \bar{\beta}_{\text{in}}\overline{S}(\omega_{\text{in}}) \\ &\times \exp[-\bar{\beta}_{\text{in}}(1-t)\bar{d}(s_i,s)]\bar{d}(s_i,s)\,\mathrm{d}t. \end{aligned} \tag{27b}$$

If $\bar{r} \geqslant \overline{R}_{\text{m}}$ (for schematic diagram, refer [7]).

(3) When no solution or $t_1,\ t_2 \notin [0,1]$

$$\begin{aligned}\bar{I}(\bar{z},\bar{r},\hat{\Omega}) &= \bar{I}_i \exp[-\bar{\beta}_{\text{out}}\bar{d}(s_i,s)] + \int_0^1 \bar{\beta}_{\text{out}}\overline{S}(\omega_{\text{out}}) \\ &\times \exp[-\bar{\beta}_{\text{out}}(1-t)\bar{d}(s_i,s)]\bar{d}(s_i,s)\,\mathrm{d}t. \end{aligned} \tag{27c}$$

(4) When only $t_2 \in [0,1]$

$$\begin{aligned}\bar{I}(\bar{z},\bar{r},\hat{\Omega}) &= \bar{I}_i \exp\left\{-[\bar{\beta}_{\text{in}} t_2 + \bar{\beta}_{\text{out}}(1-t_2)]\bar{d}(s_i,s)\right\} \\ &+ \int_0^{t_2} \bar{\beta}_{\text{in}}\overline{S}(\omega_{\text{in}}) \exp\left\{-[\bar{\beta}_{\text{in}}(t_2-t) \right. \\ &\left. +\bar{\beta}_{\text{out}}(1-t_2)]\bar{d}(s_i,s)\right\}\bar{d}(s_i,s)\,\mathrm{d}t \\ &+ \int_{t_2}^{1} \bar{\beta}_{\text{out}}\overline{S}(\omega_{\text{out}}) \\ &\times \exp[-\bar{\beta}_{\text{out}}(1-t)\bar{d}(s_i,s)]\bar{d}(s_i,s)\,\mathrm{d}t. \end{aligned} \tag{27d}$$

(5) When both $t_1,\ t_2 \in [0,1]$

$$\begin{aligned}\bar{I}(\bar{z},\bar{r},\hat{\Omega}) &= \bar{I}_i \exp\left\{-[\bar{\beta}_{\text{out}} t_1 + \bar{\beta}_{\text{in}}(t_2-t_1) \right. \\ &\left. +\bar{\beta}_{\text{out}}(1-t_2)]\bar{d}(s_i,s)\right\} + \int_0^{t_1} \bar{\beta}_{\text{out}}\overline{S}(\omega_{\text{out}}) \\ &\times \exp\left\{-[\bar{\beta}_{\text{out}}(t_1-t) + \bar{\beta}_{\text{in}}(t_2-t_1) \right. \\ &\left. +\bar{\beta}_{\text{out}}(1-t_2)]\bar{d}(s_i,s)\right\}\bar{d}(s_i,s)\,\mathrm{d}t \\ &\times \int_{t_1}^{t_2} \bar{\beta}_{\text{in}}\overline{S}(\omega_{\text{in}}) \exp\left\{-[\bar{\beta}_{\text{in}}(t_2-t) \right. \\ &\left. +\bar{\beta}_{\text{out}}(1-t_2)]\bar{d}(s_i,s)\right\}\bar{d}(s_i,s)\,\mathrm{d}t \\ &+ \int_{t_2}^{1} \bar{\beta}_{\text{out}}\overline{S}(\omega_{\text{out}}) \\ &\times \exp[-\bar{\beta}_{\text{out}}(1-t)\bar{d}(s_i,s)]\bar{d}(s_i,s)\,\mathrm{d}t. \end{aligned} \tag{27e}$$

In order to evaluate these coupled equations, 42×18 (longitudinal × radial) grids divided the domain. Subsequently, we used 80×38 grids to divide the domain for the same case. Two results had an average difference about 0.093%. Computations took about 16 h for 42×18 case, and about 70 h for 80×38 case in Digital FORTRAN 5.0 on a generic PC with 1 GB memory and an AMD Athlon™ XP 1.2 GHz processor. So the grid size 42×18 gave efficient convergence and saved significant computing time. The fluid region and porous region used different grid sizes. Piecewise second order Lagrange polynomial interpolation was assumed for the incident radiation, heat fluxes and entering intensity at the boundaries. Twenty point Gauss–Legendre quadrature was used to integrate radiative equations and line-by-line iteration method (plus TDMA) was used to solve all equations simultaneously. It was found that the solution was stable while the convergence criterion set very small (10^{-5}–10^{-8}). The values of incident radiation and heat fluxes on the boundaries were obtained by direct computation from the integrals [6,7]. The corner point values, which are the values at the intersection point of boundaries, were obtained by multidimensional extrapolation.

4. Results and discussion

In order to evaluate the enhancement of heat transfer by using the porous insert, following calculation of the dimensionless bulk temperature is necessary

$$\theta_{\text{b}} = \frac{\int_0^1 \bar{u}\theta \cdot \bar{r}\,\mathrm{d}\bar{r}}{\int_0^1 \bar{u}\bar{r}\,\mathrm{d}\bar{r}}. \tag{28}$$

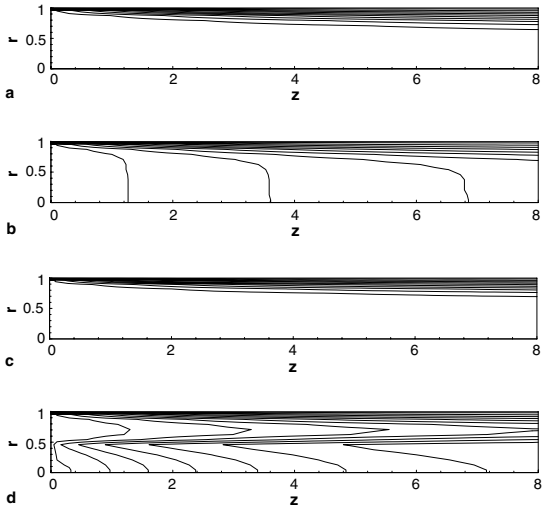

Fig. 2. Isotherms of pure convection and combined convection–radiation case, with and without the insert. $T_{\text{in}} = 1200$ K, $T_{\text{w}} = 500$ K. (a) Pure convection, $\overline{R}_{\text{m}} = 0$, $Re = 1000$; (b) Combined convection–radiation, $\overline{R}_{\text{m}} = 0$, $Re = 1000$, $\varepsilon_{\text{w}} = 0.8$, $e_1 = e_2 = 0.5$, $\beta_{\text{fluid}} = 0.5\ \text{m}^{-1}$, $\omega_{\text{fluid}} = 0$; (c) Pure convection, $\overline{R}_{\text{m}} = 0.5$, $Re = 1000$, $Da = 0.01$; (d) Combined convection–radiation, $\overline{R}_{\text{m}} = 0.5$, $Re = 1000$, $Da = 0.01$, $\varepsilon_{\text{w}} = 0.8$, $e_1 = e_2 = 0.5$, $\beta_{\text{fluid}} = 0.5\ \text{m}^{-1}$, $\omega_{\text{fluid}} = 0$, $\beta_{\text{porous}} = 200\ \text{m}^{-1}$, $\omega_{\text{porous}} = 0.8$.

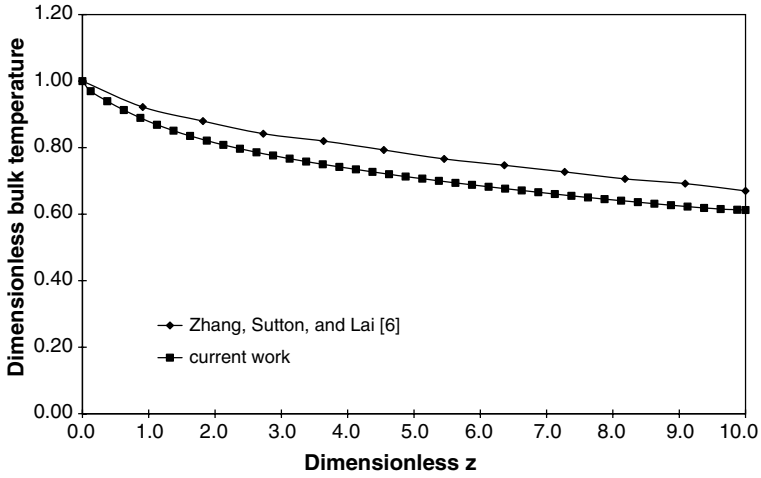

Fig. 3. The Comparison of dimensionless bulk temperature between [5] and current work, $\xi_i = 0.5$, $\tau_f = 0.01$, $\theta_w = 0.2$, $N = 0.002$ and $Pr\,Re = 4000$. The parameters are detailed in [5].

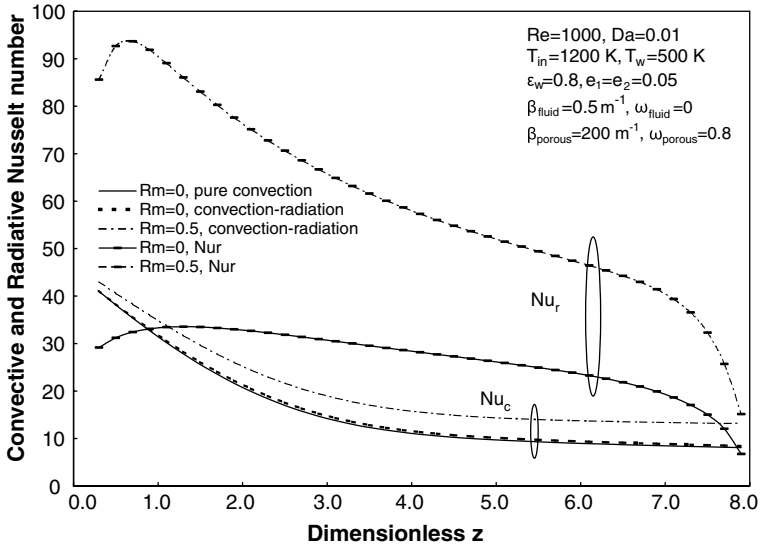

Fig. 4. Convective and radiative Nusselt number with and without the porous insert.

Table 1
The comparison for the case defined in [5] as $\xi_i = 0.5$, $\tau_f = 0.01$, $\theta_w = 0.2$, $N = 0.002$ and $Pr\,Re = 4000$ (above parameter definitions are detailed in [5])

	ξ_i	$Nu_{c,m}$	$Nu_{r,m}$	$\theta_{b,out}$
Zhang et al. [5]	0.5	14.89	22.73	0.67
Current work	0.5 ($\overline{R_m}$)	16.18	30.64	0.61

The total Nusselt number is related to the total heat flux through the cooling wall

$$Nu_T = \frac{2q_w R_{out}}{k(\theta_b - \theta_w)T_{in}}, \tag{29}$$

where,

$$q_w = q_{wc} + q_{wr}, \tag{30}$$

q_{wc}, q_{wr} are the contributions of convection and radiation respectively. They are determined by

$$q_{wc} = -\left(\frac{kT_{in}}{R_{out}}\right)\left.\frac{\partial\theta}{\partial\bar{r}}\right|_w, \quad q_{wr} = \bar{q}_r(z, R_{out}) \cdot \sigma T_{in}^4. \tag{31a, b}$$

Further,

$$Nu_c = \frac{2q_{wc}R_{out}}{k(\theta_b - \theta_w)T_{in}} = \frac{2}{(\theta_w - \theta_b)}\left.\frac{\partial\theta}{\partial\bar{r}}\right|_w,$$

$$Nu_r = \frac{2q_{wr}R_{out}}{k(\theta_b - \theta_w)T_{in}}. \tag{32a, b}$$

In order to evaluate effects of the porous insert and due to limited data in the literature, the computations are carried out on in-pipe flow with and without a porous insert. Following values are adopted: $Re = 100$–1000, $T_{in} = 1200$ K, $T_w = 500$, 800 K, $\varepsilon_w = 0.8$, 1.0, $R_{out} = 0.1$ m, $\overline{R}_m = 0, 0.2, 0.5$, $L = 0.8$ m, $Da = 10^{-4}$–1.0, $\varphi = 0.875$, $k_e = 5k_f$, $\beta_{in} = \beta_{porous} = 100$, 200, 400 m^{-1}, $\omega_{in} = \omega_{porous} = 0.5$, 0.75, 0.8, $\beta_{fluid} = 0$, 0.1, 0.5, 5 m^{-1}, $\omega_{fluid} = 0$–0.2, e_1, $e_2 = 0.05$–1.0, $a_1 = 0$, the fluid properties are assumed to be the properties of dry air at 1000 K.

In order to compare effects of the porous insert on pure convection and combined convection–radiation, temperature fields under these situations with and without the insert are shown in Fig. 2. In pure convection case, using the porous insert has forced the temperature gradient near the cooling wall to increase as illustrated in (a) and (c). So the convection is improved. In combined convection–radiation case, using the porous insert has caused the porous core temperature to drop a lot as illustrated in (b) and (d). The fluid transfers heat to the

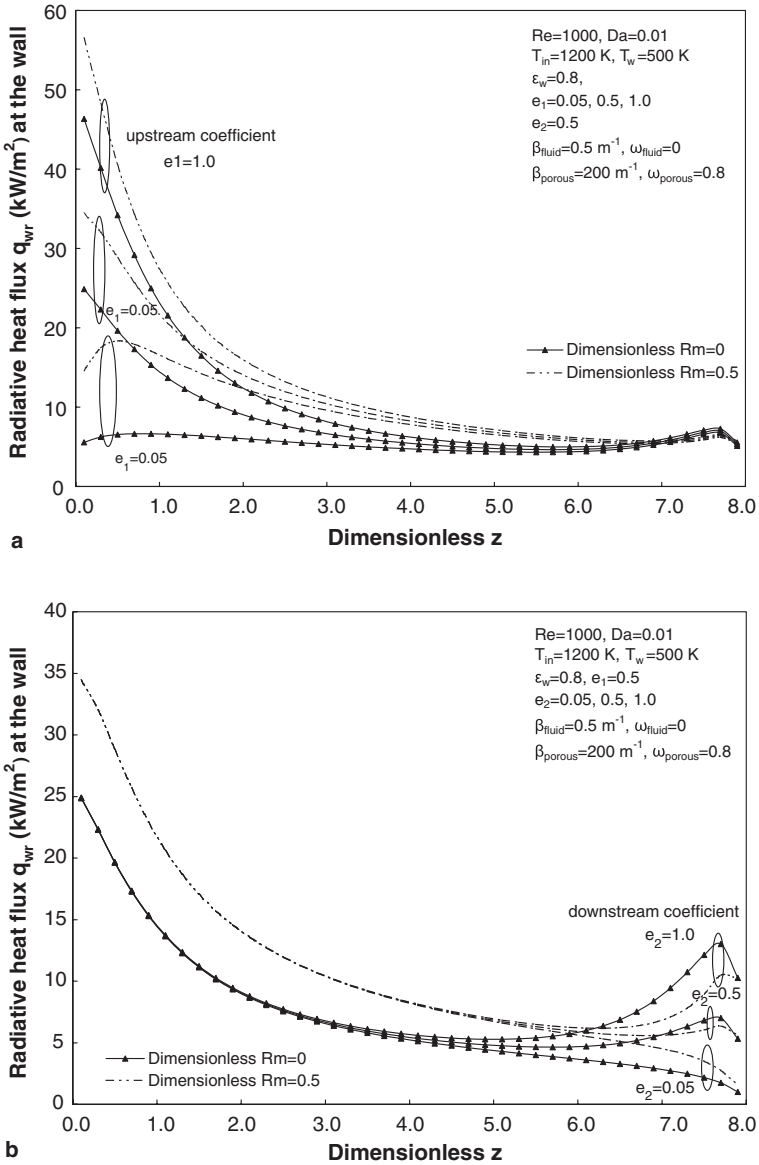

Fig. 5. Effects of externally incident radiation from upstream/downstream, $Re = 1000$, $Da = 0.01$, $T_{in} = 1200$ K, $T_w = 500$ K, $\varepsilon_w = 0.8$, $\beta_{fluid} = 0.5$ m^{-1}, $\omega_{fluid} = 0$, $\beta_{porous} = 200$ m^{-1}, $\omega_{porous} = 0.8$. (a) Radiative flux distributions with and without the insert under different coefficient e_1; (b) Radiative flux distributions with and without the insert under different coefficient e_2.

porous insert by convection; in return, the insert emits significant heat to the receiving wall by radiation.

The average bulk temperature drops along flow direction as shown in Fig. 3, which is compared with results of Zhang et al. [5]. Current dimensionless temperature is about 10% lower. This is mainly due to the fully developed velocity assumption in both porous and fluid regions by [5]. This work is simulating developing velocity. Another influence may come from the inertial term used in [5]. But this effect should be negligible [11]. The comparison of Nusselt numbers between [5] and current work is listed in Table 1. The mean radiation Nusselt number of current work is about 30% larger. In the entrance length here, more fluid pass through the porous region, so the porous insert could capture more heat from fluid by convection. The insert then emits more energy to the cold wall. The case parameters are chosen to satisfy conditions defined in [5].

The convective and radiative Nusselt numbers in the cases with and without the porous insert are shown in

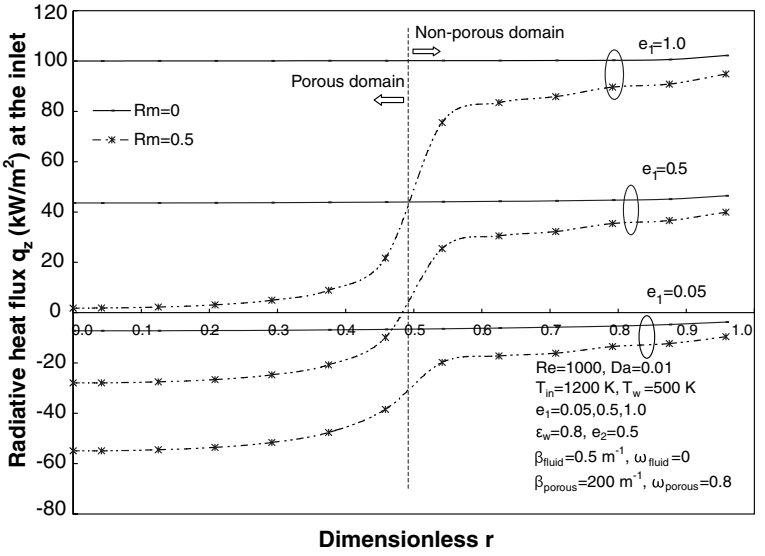

Fig. 6. The distributions of net flux component q_z at inlet under different coefficient e_1, $Re = 1000$, $Da = 0.01$, T_{in}=1200 K, $T_w = 500$ K, $\varepsilon_w = 0.8$, $\beta_{fluid} = 0.5\ m^{-1}$, $\omega_{fluid} = 0$, $\beta_{porous} = 200\ m^{-1}$, $\omega_{porous} = 0.8$.

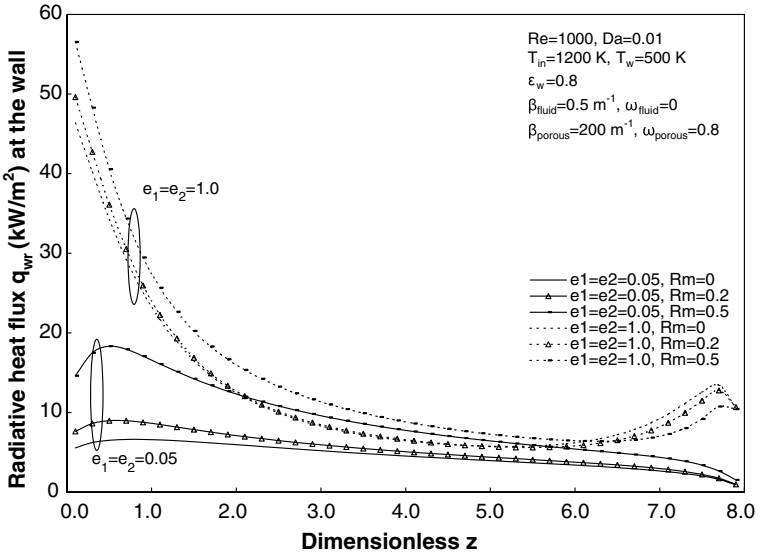

Fig. 7. Effects of the porous radius $\overline{R}_m$ on the radiative heat flux at wall under different externally incident radiation.

Fig. 4. Under combined convection–radiation situation, the convective Nusselt number will be increased by average 30% if a porous insert with $\overline{R}_m = 0.5$ is used. While the radiative Nusselt number can be increased to more than two times of that without a insert. The benefits of the insert are obvious and desirable. We will discuss the influences of some important parameters below.

4.1. The externally incident radiation

For the enhancement effect of the insert to radiative transfer, many parameters have impact on final results. The defined externally incident radiation at the inlet or outlet boundary (coefficient e_1 or e_2) has important effects on the radiative flux at the cooling wall. The effects of coefficient e_1 are shown in Fig. 5(a). For all three different e_1 values in the figure, the radiative flux at the cooling wall is enhanced greatly by using a porous insert especially near the inlet. The heat flux can be increased to approximately 1.1–2.7 times of that without an insert. This enhancement effect of the porous is stronger when e_1 is 0.05 than e_1 is 1.0. The reason is the shield effect of the porous insert to the incoming radiation from upstream, illustrated in Fig. 6. When e_1 is 1.0, a largest amount of the radiant energy comes freely into the domain if no insert installed. But with a $\overline{R}_m = 0.5$ insert, most of the radiant energy will be shielded and the total incoming energy is decreased. This shield effect of the porous insert is stronger at larger e_1. When e_1 is 0.05, the insert helps emitting more radiative energy back to the upstream.

As expected, the effects of coefficient e_2 are not as strong as that of e_1, because downstream temperature is much lower than upstream temperature after going through this cooling section. These effects of e_2 are shown in Fig. 5(b). At the smallest $e_2 = 0.05$, the heat flux q_{wr} is enhanced along the whole length by using the insert. But when e_2 is increased to 0.5 and 1.0, the heat flux q_{wr} is even lowered in a small range near the outlet. The shield effect prevents radiation returning to the domain from downstream.

4.2. The radius of the porous insert

The distributions of radiative flux at the cooling wall when $\overline{R}_m = 0.2, 0.5$ are shown in Fig. 7. At smaller coefficients $e_1 = e_2 = 0.05$, the heat flux is increased by using a $\overline{R}_m = 0.2$ insert to about 1.1–1.3 times of that without an insert, while about 1.6–2.7 times if $\overline{R}_m = 0.5$. At larger coefficients $e_1 = e_2 = 1.0$, a $\overline{R}_m = 0.2$ porous insert will force the radiative flux to be enhanced to only 1.07 times, but approximately 1.38 times if $\overline{R}_m = 0.5$. So a larger radius brings bigger enhancement effect.

4.3. Reynolds number

Reynolds number effects on the enhancement due to an insert are shown in Fig. 8. The enhancement of the radiative flux is increased with Reynolds number. Under parameters stated in the figure and $Re = 1000$, the radiative flux could be increased to about 1.1–1.38 times of that in clear flow, while only about 1.03–1.2 times if $Re = 100$.

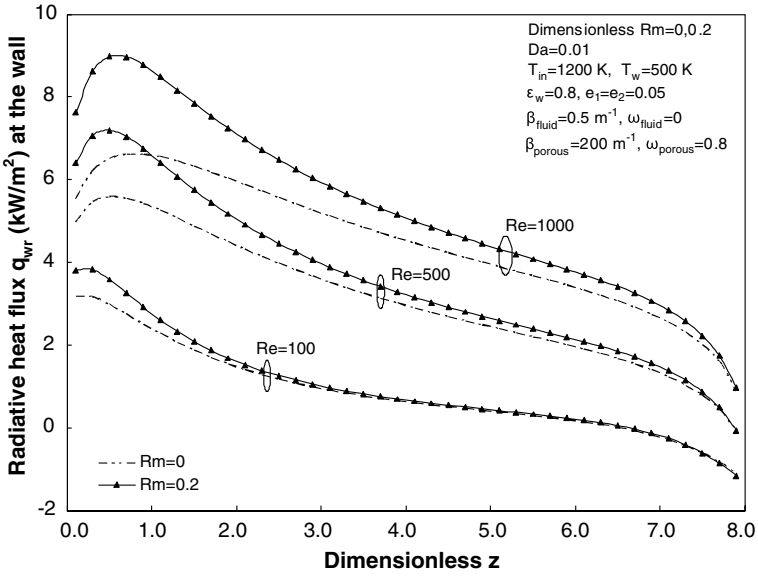

Fig. 8. Effects of the porous insert under different Reynolds numbers.

4.4. The properties of the porous insert

The effects of the scattering albedo of the porous insert on radiative transfer are shown in Fig. 9(a). A smaller albedo causes larger radiative energy transferred to the cooling wall. As expected, this effect is increased if the radius of the insert is increased. The extinction coefficient of the insert has significant effect on the enhancement as shown in Fig. 9(b). Increasing the extinction coefficient has the same effect as decreasing the scattering albedo. Larger extinction coefficient brings bigger enhancement effect, especially near the inlet. As the extinction coefficient is increased from $200\,m^{-1}$ to $400\,m^{-1}$, the radiative flux can be increased to about 1.06–1.09 times by using a $\overline{R}_m = 0.2$ insert, and about 1.15–1.5 times for $\overline{R}_m = 0.5$. Choosing porous material with small scattering albedo and large extinction coefficient for the insert should enhance heat transfer.

4.5. Darcy number Da

The effects of Darcy number are important for all porous materials. The developing profiles of the flow field at $Da = 0.01$ and 0.001 are shown in Fig. 10(a)

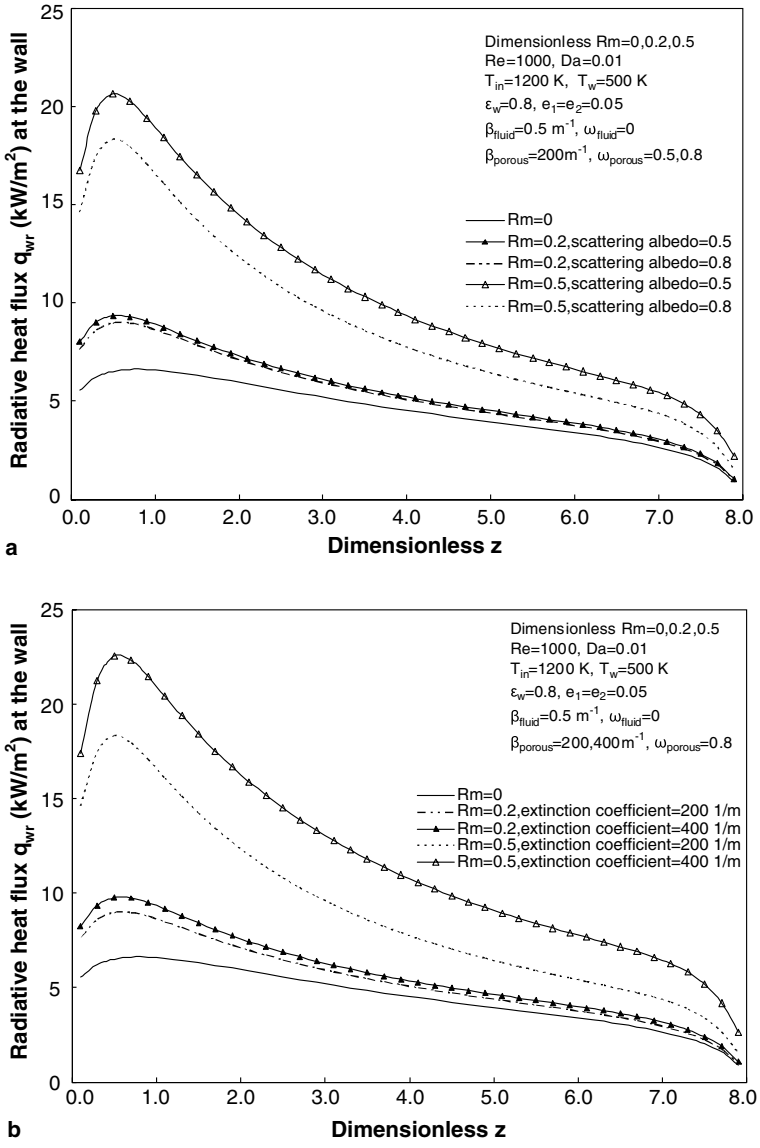

Fig. 9. Effects of porous properties on the radiative heat flux at wall: (a) radiative flux under different porous scattering albedo and (b) radiative flux under different porous extinction coefficients.

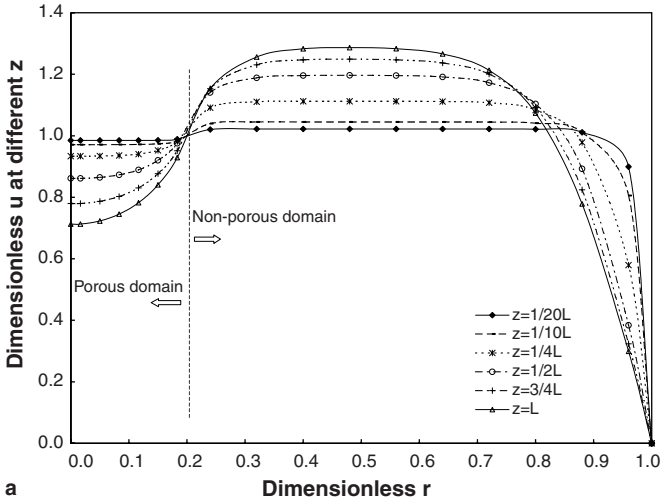

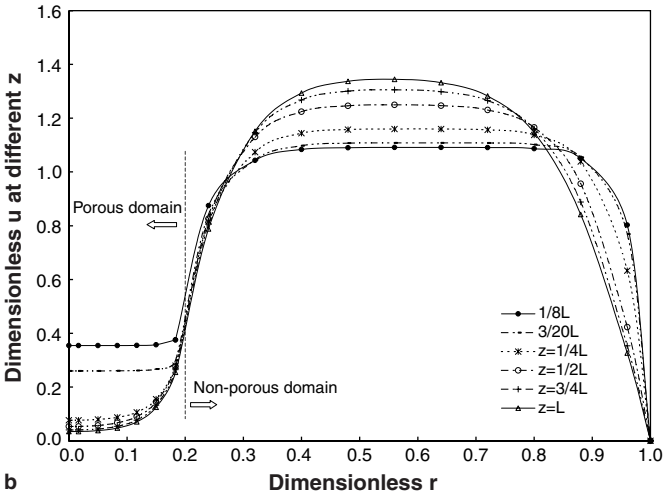

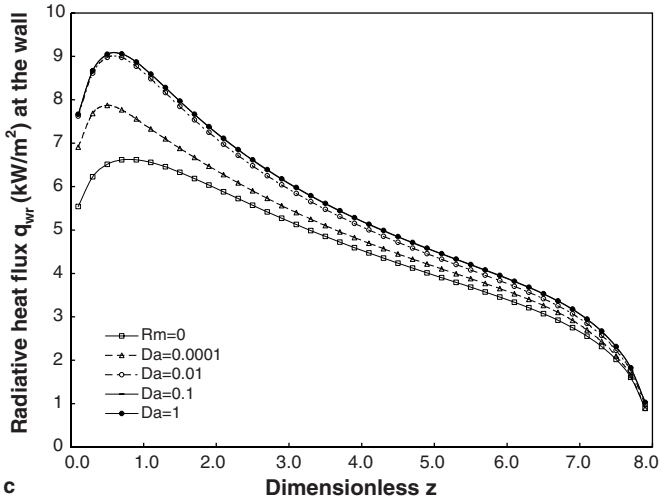

Fig. 10. Effects of Darcy number, $\overline{R}_m = 0.2$, $Re = 1000$, T_{in}=1200 K, $T_w = 500$ K, $\varepsilon_w = 0.8$, $e_1 = e_2 = 0.05$, 0.5, $\beta_{fluid} = 0.5\ m^{-1}$, $\omega_{fluid} = 0$, $\beta_{porous} = 200\ m^{-1}$, $\omega_{porous} = 0.8$. (a) Velocity developing profiles when $Da = 0.01$, $e_1 = e_2 = 0.5$; (b) Velocity developing profiles when $Da = 0.001$, $e_1 = e_2 = 0.5$; (c) Radiative flux at the cooling wall at different Da, $e_1 = e_2 = 0.05$.

and (b) respectively. It is interesting to note that when the fluid flows in z-direction, some of the fluid will flow from the porous domain to the clear domain. So, the velocity in the clear domain increases, while the velocity in the porous domain decreases. The mass flow rate in the porous domain increases with Darcy number when fully developed.

The effects of Darcy number on the radiative transfer are illustrated in Fig. 10(c). Increasing Darcy number will enhance the heat transfer. When Darcy number is increased from 0.0001 to 0.01, the radiative flux increases from 1.05–1.23 times to 1.10–1.38 times of clear flow. This is because the convection inside porous media is improved under large Darcy number, so more energy in fluid can be captured and transferred out in radiation. But if Darcy number is further increased from 0.01 to 0.1, the radiative flux increases little. The heat flux of Darcy number 1.0 remains approximately the same as Darcy number 0.1.

Large Darcy number will benefit the radiative transfer enhancement, but the value of *Da* is normally much less than unity. Weinert and Lage [14] in 1994 reported a sample of compressed aluminum foam of 1 mm thick, which has a *Da* number about 8 and is 'hyper-porous medium'. Cordierite ceramic foam (manufactured by Bridgestone Tyre Co. Ltd) was made into a plate sample

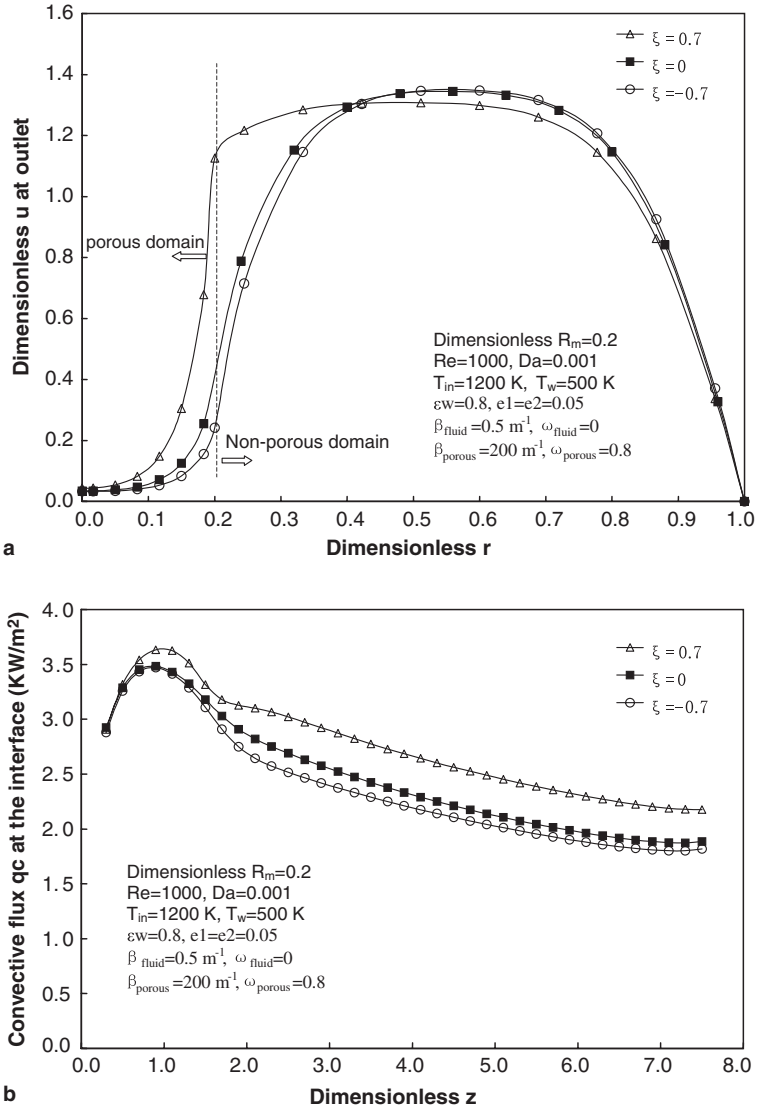

Fig. 11. Effects of parameter ξ on flow and heat transfer in the interfacial region. (a) Velocity distributions at outlet under different ξ; (b) Convective heat flux at the interface under different ξ.

and investigated by Kamiuto etc. [15], properties are: porosity = 0.879, pore diameter = (2.82–6.35) × 10^{-3} m, extinction coefficient = 212.3 m^{-1}, and albedo of about 1.0. By using Kozeny's equation, permeability is calculated as 1.04×10^{-5} m^2. Darcy number is 1.04×10^{-3}. From the radiative transfer and pressure drop point of view, the bigger *Da* number the better. In this work, properties of porous medium are approximate to cordierite.

4.6. Parameter in the stress jump condition

The stress jump condition provided by [9] is

$$\frac{\partial u_{\text{fluid}}}{\partial r} = \varphi^{-1} \frac{\partial u_{\text{porous}}}{\partial r} - \frac{\xi}{\sqrt{K}} u_{\text{porous}}, \tag{33}$$

where the parameter ξ is of order one predicted by the theory. It could be positive or negative. The effects of positive and negative ξ are shown in Fig. 11(a) and (b). The velocity distributions at the outlet are shown in (a). In the area close to the interface, more fluid flow through when $\xi = 0.7 > 0$, while less fluid flow through when $\xi = -0.7 < 0$. The convection heat flux at the interface is shown in (b). Larger parameter ξ enhances convection at the interface.

5. Conclusions

In this paper, a combined convective–radiative heat transfer computation scheme is proposed and used to solve combined problems, with and without the porous core. Radiation in a two-layer non-homogeneous participating medium is solved by newly developed transformed integral equations. With the insert, the radiative transfer and convective heat transfer are both enhanced. With a $\overline{R}_{\text{m}} = 0.5$ porous insert, the convective Nusselt number can be increased up to 35% and the radiative Nusselt number can be increased up to 105%. The porous insert has a shield effect to the incoming externally incident radiation both from upstream and downstream. This shield effect of the porous medium emitting radiation more back to the upstream direction is desirable in some energy systems. The heat transfer enhancement to the cooling wall is larger under a bigger radius of the insert and a faster velocity. The large extinction coefficient and small scattering albedo of the porous material benefit the enhancement of heat transfer. Using the porous insert in optical thick working gas has relatively little effect of the enhancement. Increasing Darcy number of the porous insert will also increase this enhancement effect.

References

[1] Y. Mori, T. Taira, K. Watanabe, Heat exchanger augmentation by radiation plates, in: Proceedings of the ASME–AIChE National Heat Transfer Conference, St. Louis, Missouri, August 1976, ASME Paper No. 76-HT-3.
[2] M. Hirano, T. Miyauchi, Y. Takahira, Enhancement of radiative heat transfer in the laminar channel flow of non-gray gases, Int. J. Heat Mass Transfer 31 (2) (1988) 367–374.
[3] H.Y. Zhang, M.A. Ebadian, Convective–radiative heat transfer in the thermal entrance region of the semicircular duct with streamwise internal fins, Int. J. Heat Mass Transfer 34 (12) (1991) 3135–3142.
[4] R. Echigo, Effective energy conversion method between gas enthalpy and thermal radiation and application to industry furnaces, in: Proceedings of the 7th International Heat Transfer Conference, Munich, vol. 6, September 1982, pp. 361–366.
[5] J.M. Zhang, W.H. Sutton, F.C. Lai, Enhancement of heat transfer using porous convection-to-radiation converter for laminar flow in a circular duct, Int. J. Heat Mass Transfer 40 (1) (1997) 39–48.
[6] X.L. Chen, W. Sutton, Radiative transfer in finite cylindrical media using transformed integral equations, J. Quant. Spectrosc. Radiat. Transfer 77 (3) (2003) 233–271.
[7] W. Sutton, X.L. Chen, A general integration method for radiative transfer in 3-D non-homogeneous cylindrical media with anisotropic scattering, J. Quant. Spectrosc. Radiat. Transfer 84 (2004) 65–103.
[8] M. Kaviany, in: Principles of Heat Transfer in Porous MediaMechanical Engineering Series, Springer-Verlag, New York, 1991.
[9] J. Alberto Ochoa-Tapia, S. Whitaker, Momentum transfer at the boundary between a porous medium and a homogeneous fluid—I. Theoretical development, Int. J. Heat Mass Transfer 38 (14) (1995) 2635–2646.
[10] J. Alberto Ochoa-Tapia, S. Whitaker, Momentum transfer at the boundary between a porous medium and a homogeneous fluid—II. Comparison with experiment, Int. J. Heat Mass Transfer 38 (14) (1995) 2647–2655.
[11] M.K. Alkam, M.A. Al-nimr, Transient non-Darcian forced convection flow in a pipe partially filled with a porous material, Int. J. Heat Mass Transfer 41 (2) (1998) 347–356.
[12] S.V. Patankar, Numerical Heat Transfer and Fluid Flow, Hemisphere Publishing Corporation, Washington, New York, London, 1980.
[13] M.N. Ozisik, Radiative Transfer and Interactions with Conduction and Convection, Wiley, New York, NY, 1973.
[14] A. Weinert, J.L. Lage, Porous aluminum-alloy based cooling devices for electronics, SMU-MED-CPMA Inter. Rep. 1.01/94, Southern Methodist University, Dallas, TX [1.5.3].
[15] K. Kamiuto, M. Sato, M. Iwamoto, Determination of the radiative properties of high-porosity materials by use of the emerging-intensity fitting method, J. Quant. Spectrosc. Radiat. Transfer 42 (6) (1989) 477–482.